Published in final edited form as:
J Micromech Microeng. 2009 July 1; 19(7): 1–6. doi:10.1088/0960-1317/19/7/075012.

Hierarchical self-assembly of complex polyhedral microcontainers

David J. Filipiak[1,4], **Anum Azam**[2,4], **Timothy G. Leong**[1], and **David H. Gracias**[1,3,5]

[1] Department of Chemical and Biomolecular Engineering, The Johns Hopkins University, Baltimore, Maryland 21218

[2] Department of Biomedical Engineering, The Johns Hopkins University, Baltimore, Maryland 21218

[3] Department of Chemistry, The Johns Hopkins University, Baltimore, Maryland 21218

Abstract

The concept of self-assembly of a two-dimensional (2D) template to a three-dimensional (3D) structure has been suggested as a strategy to enable highly parallel fabrication of complex, patterned microstructures. We have previously studied the surface tension based self-assembly of patterned, microscale polyhedral containers (cubes, square pyramids and tetrahedral frusta). In this paper, we describe the observed hierarchical self-assembly of more complex, patterned polyhedral containers in the form of regular dodecahedra and octahedra. The hierarchical design methodology, combined with the use of self-correction mechanisms, was found to greatly reduce the propagation of self-assembly error that occurs in these more complex systems. It is a highly effective way to mass-produce patterned, complex 3D structures on the microscale and could also facilitate encapsulation of cargo in a parallel and cost-effective manner. Furthermore, the behavior that we have observed may be useful in the assembly of complex systems with large numbers of components.

1. Introduction

Hierarchical assembly is a strategy developed in nature to construct essential biomolecules, such as proteins and nucleic acids [1–4]. In natural self-assembly, hierarchy is enabled by a variety of bonds such as covalent, electrostatic, and hydrogen bonds, as well as the range of length scales [5–6]. For example, viral capsid proteins self-assemble into complex polyhedral biological containers. Icosahedral capsids are seen commonly among viruses such as the herpes virus [7]. Dodecahedral particles have been observed to assemble from mutant adenovirus capsid proteins [8] and from duplex RNA cages around the icosahedral capsid of the Pariacoto virus [9]. These geometries approach spherical morphologies and are advantageous due to their inherent maximization of volume to surface area ratios. Viruses that adopt complex polyhedral geometries are thereby able to maximize the amount of viral genetic information contained within minimized surface areas [10]. Moreover, polyhedral shapes that approach spheres have larger internal angles (as compared to cubes or tetrahedra). For drug delivery or lab-on-a-chip

5Corresponding Author. E-mail: dgracias@jhu.edu; Phone: 410-516-5284, The Johns Hopkins University, 3400 North Charles Street, Baltimore, Maryland 21218.

[4]These authors contributed equally to this work.

Videos featuring a schematic animation and real-time folding of a 500μm dodecahedral container. This material is available free of charge via the Internet at http://

applications in particular, such shapes result in a more streamlined object, thereby minimizing drag in the surrounding fluidic medium [10].

While the fabrication of unpatterned polyhedral particles has been elegantly demonstrated [11–15], it is extremely challenging to construct such polyhedra with any desired surface patterning of panels. Arbitrary patterning of polyhedral panels may be useful for increasing and customizing the functionality of these microscale containers for a wide range of applications in packaging, drug delivery and cell therapy. Conventional micropatterning is an inherently 2D process and novel 3D fabrication strategies, such as stereolithography, are essentially serial methods [16]. In this work, we demonstrate parallel assembly of hollow octahedra and regular dodecahedra from 2D tethered panels (referred to as nets) to 3D structures using a hierarchical self-assembly approach. We denote hierarchical self-assembly to involve a series of sequential steps whereupon subunits first form and then lead to the assembly of the final structure. While we have previously studied the self-assembly of simpler, microscale polyhedral containers [17], those geometries assembled from nets with fewer panels as compared to the more complex polyhedra described in this work, namely the octahedron (the net has 8 panels) and dodecahedron (the net has 12 panels). Moreover, prior fabrication methods did not involve a multi-step self-assembly process.

Self-assembly is often associated with the emergence of order from a disordered collection of precursor components. In the case of polyhedral self-assembly from panels, it is extremely unlikely that a system composed of un-tethered panels would result in an ordered polyhedron (figure 1(a)). Hence, in our laboratory we have tethered the panels together (figure 1(b)) to limit the number of possible self-assembly outcomes. Tethering limits the degrees of freedom of interacting panels and minimizes the range of energetically favorable self-assembly configurations. Nevertheless, panels can be tethered in a large number of ways, especially for higher-order polyhedra, and limited *a priori* guiding principles exist for choosing nets that assemble with the highest yield of desired self-assembled structures. Recently, we found that 2D cubic and octahedral nets that are more compact yielded larger numbers of perfect, self-assembled cubes and octahedra [18]. In this paper, we explore the importance of hierarchy inherent in the sequential steps required to self-assemble more complex tethered panels into the final structures. Additionally, we describe the self-correction and cooperativity that occurs during this assembly, a result of the locking mechanisms in our design.

2. Experimental details

The nets for the more complex polyhedra consisted of pentagonal (for dodecahedra) and triangular (for octahedra) panels tethered by solder hinges; the panels and hinges were patterned using conventional photolithography and fabricated using electrodeposition. This fabrication process was carried out in two similar steps. First, panels were patterned and electrodeposited with nickel (Ni). Two distinct types of hinges were then patterned and fabricated in a second step: internal “folding” hinges that tether panels together and lift them out of plane and half-width “locking” hinges that surround the outer panels and seal the edges of the final 3D structure [17,19]. Both sets of hinges were composed of electrodeposited 60/40 tin/lead solder. We used our previously-established process [17] to achieve self-assembly by melting the hinges of the 2D templates in a high boiling point solvent (N-methylpyrrolidone). The design of the folding hinge is described in figure 1(b). The minimization of the surface tension of the liquefied solder resulted in a torque that caused the hinges to ball up and rotated the panels upward [19]. Simultaneously, the molten solder in the locking hinges fused together as they minimized their surface area exposed to the surrounding fluid [20]. The design of the locking hinge and fusion process is described in figure 1(c).

There are 43,380 different 2D nets that can assemble into a regular dodecahedron [21]. From this large number of possible nets, we chose one with a central axis and two identical halves (figure 2(a)). It could also be easily visualized that this net would assemble in a hierarchical fashion. The octahedron has 11 different 2D nets, several of which are geometrically capable of folding into either of two different configurations: regular or concave irregular (boat) [18]. Here, we focused on the net (figure 2(b)) that had a folding pattern that clearly demonstrated hierarchical self-assembly and could self-assemble into either configuration.

3. Results and discussion

Previously, we described simulations that demonstrated that the angle through which the panels rotated depended on the volume of solder deposited in the internal folding hinge [17]. Theoretically for a given hinge design, there is an ideal solder volume correlating to a specific folding angle, and positive or negative deviations from that can lead to under or over folding, respectively. However, the effect of the external locking hinges was not captured in the model. We have observed that these locking hinges enhance the assembly yields as they compensate (to some extent) for the deviations that may occur in folding angle of the internal hinge. One could conceivably fold perfect structures without the locking hinges; however, the hinge dimensions would need to be very accurately targeted for the desired internal angles.

In this work, we performed control studies in which various solder volumes, corresponding to different solder heights, were electrodeposited on identical 500 μm (panel edge length) 2D templates to determine the corresponding fold angle, while also taking into account the effect of the locking hinges. For fabricating dodecahedra, hinge dimensions used to achieve the 90° fold angle for cubes [17,22] resulted in over-folding of panels for dodecahedra (figure 3(a)). Steric hindrances between panels then prevented the net from assembling into dodecahedra. We empirically tested different solder heights to obtain the proper folding angle, which for the regular dodecahedra is approximately 63.4°. We determined height dimensions by measuring the solder hinge heights using profilometry. Over-folding of panels occurred with approximate solder hinge heights of 15 μm and 24 μm (figures 3(a) and (b)), while the greatest yield of structures with correct folding angles was observed with a hinge height of 28 μm (figure 3(c)). Under-folding occurred more commonly with solder hinge heights of 34 μm and greater (figure 3(d)). Thus, the recommended solder height for the fabrication of 500 μm scale regular dodecahedron with our hinge design was approximately 28 μm and increased linearly with increasing polyhedra size. It is important to note that in our control experiments, well-folded polyhedra did assemble at each hinge test height; however, the test height of ~28 μm resulted in the greatest *yield* of well-folded polyhedra.

We fabricated two types of test structures to specifically determine the effect of the locking hinges for a given folding hinge height of 28 μm. Using the regular dodecahedron net, the central hinge between the panels labeled “3” in figure 2(a) was removed resulting in two half-dodecahedral structures. The other folding hinges were present in both test structures, but the locking hinges were removed from one of the test structures. A clear trend was observed when self-assembling the structures; those without locking hinges often resulted in over-folded and misaligned panels, whereas those with the locking hinges tended to fold as desired. The contact between two adjacent molten locking hinges provided self-alignment [23] and could correct for defects in folding angle. We also observed that many hinges often corrected at once in a cooperative manner.

The assembly of octahedra and regular dodecahedra occurred with a series of successive hierarchical steps as depicted in figure 2. The dynamics of regular dodecahedron self-assembly, captured during the self-assembly of a single dodecahedron, are shown in figure 4. Initially, both halves folded independently in two steps and at approximately equal rates (figures 4(a),

(b), and (c)). The two halves then approached each other in the final step. Occasionally, some hinges melted before others resulting in unsynchronized folding of panels. However, a remarkably high level of cooperativity in self-correction was observed in the final steps. This is evident in the image sequence in figures 4(d), (e), and (f). In figure 4(d) it appears as though a defective dodecahedron would result, since the two halves have folded to different extents and have slightly misaligned edges; however, once the outer locking hinges came in contact with each other, the structure adjusted its configuration (figures 4(d) and (e)) to form a perfect regular dodecahedron (figure 4(f)). An explanation for the observed self-correcting phenomenon is that liquefied locking hinges made contact with each other and effectively held the two halves in close proximity until all of the panels folded to the desired angle; at this point, the fabrication of the regular dodecahedron was complete. A 500 μm (panel edge length) regular dodecahedron patterned differently on each panel and a collection of many 100, 200, and 500 μm regular dodecahedra demonstrate process versatility (featured in figures 5(a) and (b), respectively).

The folding mechanics observed during octahedron fabrication followed a similar pattern of hierarchical self-assembly. However, depending on how the edge-to-edge connections were formed as the octahedron folded, we found that the same 2D net was geometrically capable of hierarchically assembling into either the regular or irregular (boat) configuration. The folding sequence of the octahedron net was identical in both cases, but the panels attached at different locations to form the two configurations (figures 5(c) and (d)). Process and patterning versatility were also demonstrated with the octahedra for sizes ranging from 200–500 μm, as featured in figure 5(e).

We believe that the hierarchical folding order occurs as a result of modules of smaller size (and weight) folding before those of larger size (and weight). It should be noted that the composition and dimensions of all hinges within a particular net were the same. Hence, the surface tension force generated at each hinge was the same. However, when the net was flat, the opposing gravitational torque at hinge 1 was much smaller as compared to that at hinge 2 and 3. For dodecahedra, the edge length of a single panel was 100, 200, or 500 μm, but the size scale of the whole 2D net for the variously sized dodecahedra fell into the range of approximately 1–4 mm. We observed that single panels denoted by “1” in figure 2 fold first, followed by the panels denoted by “2” in figure 2, and finally by the panels labeled as “3”. This hierarchical folding order was common among 100, 200, and 500 μm dodecahedra. Previous research has shown that even though gravitational effects are negligible at small size scales (sub-mm), they begin to play a more significant role in mm-scale structures [17,22,24,25]. We note that the surface tension-driven folding was opposed by gravity since we positioned the nets with the solder facing upwards and away from the bottom of the glass dish immediately prior to assembly. When the solder faced downward, structures were more likely to assemble with defects, since the molten solder can become deformed by the glass bottom. There is a subsequent difference in the dynamics based on size i.e. structures with smaller size (and weight) fold before those with greater size (and weight), and this explains the particular folding sequence of the panels in the octahedra and regular dodecahedra. Our previous analysis explored the effect of size scaling on surface tension versus inertial forces from a thermodynamic perspective (to determine self-folding spontaneity based on equilibrium states), but it could not capture the dynamics of the process. Therefore, in this system where self-assembly is spontaneous, both surface tension forces and gravitational forces played a role in the dynamics of the assembly. The final structure of the polyhedra was thus dependent on the particular steps in the assembly process.

The locking hinges were critical in enabling the cooperativity and significant defect tolerance observed. When edges of adjacent panels met during assembly, the liquid solder of the locking hinges on adjacent panels coalesced. Consequently, these hinges worked in a cooperative

manner to achieve the final assembly. The dodecahedron net we chose for our design had outer panels with four locking hinge coalescence sites around each panel. Two of these locking hinges, oriented radially outward from the center of each half of the dodecahedron, increased the probability that locking hinges on adjacent panels would meet, effectively averaging out the small variations in folding angles and timing of folds. The other two locking hinges were responsible for interacting with the other half of the dodecahedra during the final assembly step. We observed that initial yields for the un-optimized self-assembly of octahedra and dodecahedra were ~30% and ~25%, respectively. Compared to our previous work, yields were expected to be lower for increasingly complex polyhedra, as additional panels compound the likelihood of patterning and assembly errors. However, it is again important to note that due to the presence of the locking hinges, we were able to successfully self-assemble dodecahedra with all of the various tested hinge solder heights. It was the overall yields that changed accordingly with the heights of the folding hinges, and we are continuing to optimize the process to increase yields for complex polyhedra.

By utilizing self-assembly in conjunction with photolithography, we have facilitated parallel mass-production of hollow 3D structures with individually-patterned panels, as well as with anisotropic patterning (figure 5(a)). Our process is additionally versatile in that it is possible to simultaneously encapsulate cargo, such as glass beads, during the assembly process. We encapsulated ~128 μm and 275 μm diameter glass beads (figure 5(f)) within 200 and 500 μm regular dodecahedra, respectively, by assembling the polyhedral containers in the presence of the beads. This demonstration of encapsulation of cargo is a primary step in the realization of utilizing polyhedra for microscale packaging applications.

4. Conclusion

In conclusion, we have demonstrated a strategy to construct complex hollow, patterned, microscale polyhedra using a hierarchical self-assembly approach. Furthermore, our folding process has been found to work in more complex systems, using the highly effective self-correcting mechanisms of the locking hinges. We have designed and observed the order in which these relatively complex structures fold and believe that the utilization of this behavior may be useful for the design of future self-assembling systems, particularly those of increasing complexity. A major challenge in designing self-assembling systems is to minimize errors; this hierarchical design method is an effective approach to reduce error propagation during the assembly of complex systems. Additionally, the corrective action exhibited by the locking hinges further reduces error, especially in the final stages of assembly.

We envision the use of these complex structures in lab-on-a-chip applications, as vehicles for drug delivery, and as 3D electromagnetic components. Higher order polyhedral morphologies, such as the dodecahedron, are especially desirable for lab-on-a-chip and drug delivery applications with maximized container volume/surface area ratios and reduced drag. Thus, a good methodology to fabricate such higher-order polyhedral structures is needed. Though we have demonstrated this strategy only with metallic structures, photolithographic patterning is versatile. This strategy can be used to create structures with other material combinations and additionally allow integration of dissimilar materials on the panels. The fabrication scheme outlined in this work is also CMOS compatible which will enable the incorporation of electronic modules, sensors, and actuators on or within the polyhedral containers. This trait would further enhance functionality for lab-on-a chip and drug delivery applications, and it provides a new method for developing 3D electromagnetic building blocks that can in turn be used in increasingly hierarchical self-assembly.

Supplementary Material

Refer to Web version on PubMed Central for supplementary material.

Acknowledgments

This work was supported by grants from the National Science Foundation (Career-DMMI 044816) and by the NIH Director's New Innovator Award Program, part of the NIH Roadmap for Medical Research, through grant number 1-DP2-OD004346-01. Information about the NIH Roadmap can be found at http://nihroadmap.nih.gov

References

1. Uzawa T, Nishimura C, Akiyama S, Ishimori K, Takahashi S, Dyson JH, Wright PE. Collapse and search dynamics of apomyoglobin folding revealed by submillisecond observations of alpha-helical content and compactness . Proc Natl Acad Sci USA 2008;105:13859–13864. [PubMed: 18779573]
2. Jabbari H, Condon A, Zhao S. Novel and efficient RNA secondary structure prediction using hierarchical folding . J Comput Bio 2008;15:139–163. [PubMed: 18312147]
3. Shcherbakova I, Brenowitz M. Perturbation of the hierarchical folding of a large RNA by the destabilization of its scaffold's tertiary structure . J Mol Bio 2005;354:483–496. [PubMed: 16242711]
4. Yeh S, Ropson IJ, Rousseau DL. Hierarchical folding of intestinal fatty acid binding protein . Biochemistry 2001;40:4205–4210. [PubMed: 11284675]
5. Compiani M, Capriotti E, Casadio R. Dynamics of the minimally frustrated helices determine the hierarchical folding of small helical proteins . Phys Rev E 2004;69:51905.1–51905.8.
6. Fürtig B, Buck J, Manoharan V, Bermel W, Jäschke A, Wenter P, Pitsch S, Schwalbe H. Time-resolved NMR studies of RNA folding . Biopolymers 2007;86:360–383. [PubMed: 17595685]
7. Cardone G, Winkler DC, Trus BL, Cheng N, Heuser JE, Newcomb WW, Brown JC, Steven AC. Visualization of the herpes simplex virus portal in situ by cryo-electron tomography . Virology 2007;361:426–434. [PubMed: 17188319]
8. Fuschiotti P, Fender P, Schoehn G, Conway JF. Development of the dodecahedral penton particle from adenovirus 3 for therapeutic application . J Gen Virol 2006;87:2901–2905. [PubMed: 16963748]
9. Tang L, Johnson KN, Ball A, Lin T, Yeager M, Johnson JE. The structure of Pariacoto virus reveals a dodecahedral cage of duplex RNA . Nat Struct Mol Biol 2001;8:77–83.
10. Freitas, RA, Jr. Nanomedicine. Vol. Chapter 5. Landes Bioscience; Georgetown, TX: 1999. p. 123-124.
11. Chen F, Gao Q, Hong G, Ni J. Synthesis and characterization of magnetite dodecahedron nanostructure by hydrothermal method . J Magn Magn Mater 2008;320:1775–1780.
12. Montejano-Carrizales JM, Rodríguez-López JL, Pal U, Miki-Yoshida M, José-Yacamán M. The completion of the platonic atomic polyhedra: the dodecahedron . Small 2006;2:351–355. [PubMed: 17193048]
13. Zhang Q, Xie J, Lee JY, Zhang J, Boothroyd C. Synthesis of Ag@AgAu metal core/alloy shell bimetallic nanoparticles with tunable shell compositions by a galvanic replacement reaction . Small 2008;4:1067–1071. [PubMed: 18651712]
14. Xu H, Wang X, Zhang L. Selective preparation of nanorods and micro-octahedrons of Fe2O3 and their catalytic performances for thermal decomposition of ammonium perchlorate . Powder Technol 2008;185:176–180.
15. Zhang J, Liu H, Wang Z, Ming N. Shape-selective synthesis of gold nanoparticles with controlled sizes, shapes, and plasmon resonances . Adv Funct Mater 2007;17:3295–3303.
16. Hull CW. US Patent 4 575 330. 1986
17. Leong TG, Lester PA, Koh TL, Call EK, Gracias DH. Surface tension-driven self-folding polyhedra . Langmuir 2007;23:8747–8751. [PubMed: 17608507]
18. Azam A, Leong TG, Zarafshar AM, Gracias DH. Compactness determines the success of cube and octahedron self-assembly . PLoS ONE 2009;4 :e4451. [PubMed: 19212438]
19. Syms RRA. Equilibrium of hinged and hingeless structures rotated using surface tension forces . J Microelectromech Syst 1995;4:177–184.

20. Gracias DH, Tien J, Breen TL, Hsu C, Whitesides GM. Forming electrical networks in three dimensions by self-assembly . Science 2000;289:1170–1172. [PubMed: 10947979]

21. Bouzette S, Buekenhout F, Dony E, Gottcheiner A. A theory of nets for polyhedra and polytopes related to incidence geometries . Des Codes Cryptography 1997;10:115–136.

22. Syms RRA. Surface tension powered self-assembly of 3-D micro-optomechanical structures . J Microelectromech Syst 1999;8:448–454.

23. Jacobs HO, Tao AR, Schwartz A, Gracias DH, Whitesides GM. Fabrication of a cylindrical display by patterned assembly . Science 2002;296:323–325. [PubMed: 11951039]

24. Wautelet M. Scaling laws in the macro-, micro- and nanoworlds . Eur J Phys 2001;22:601–611.

25. Hoyle CD, Kapner DJ, Heckel BR, Adelberger EG, Gundlach JH, Schmidt U, Swanson HE. Submillimeter tests of the gravitational inverse-square law . Phys Rev D 2004;70:042004.

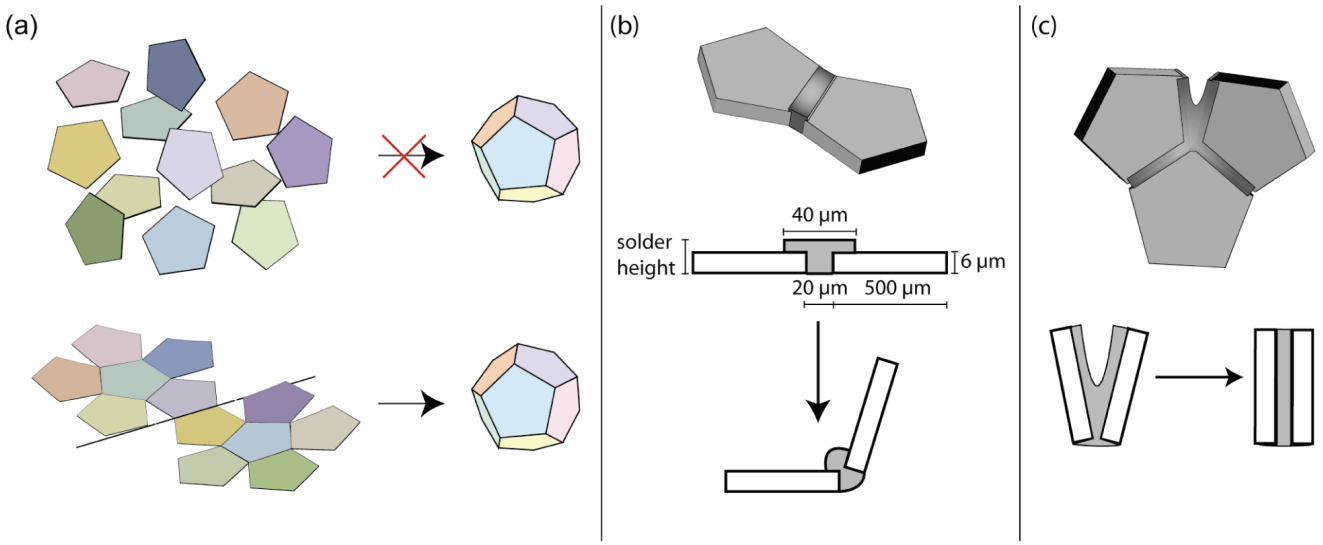

Figure 1.
(a) It is highly improbable that 12 free-floating panels will self-assemble to form a dodecahedron. Tethering limits the number of possible self-assembly outcomes and can be used to construct a dodecahedron. (b–c) The two types of hinges used; both hinges work due to a minimization of surface energy. (b) Internal folding hinges cause panels to torque while (c) external locking hinges help self-align panel edges and seal the structure.

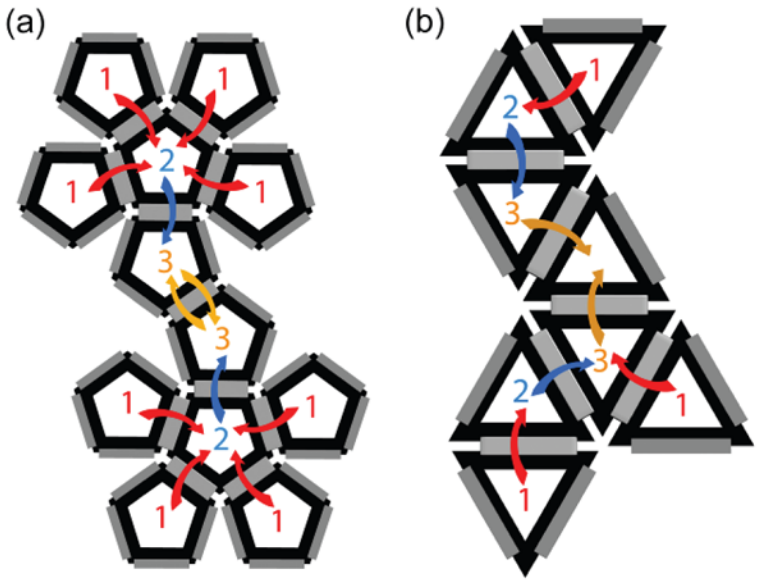

Figure 2. Schematics of the nets (tethered panels and hinges) used for the hierarchical self-assembly of (a) the dodecahedron and (b) octahedron

The numbers in the figure indicate the folding sequence of the panels.

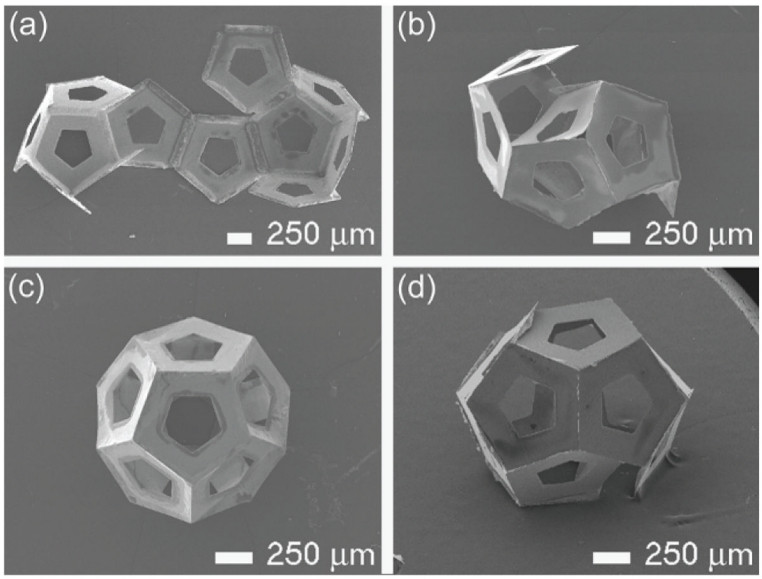

Figure 3. SEM images of results from control study determining fold angle as a function of solder hinge height

Panels (a–d) show dodecahedra folded with different hinge volumes: (a) 15 μm (over-folded); (b) 24 μm (over-folded); (c) 28 μm (correctly folded); and (d) 34 μm (under-folded).

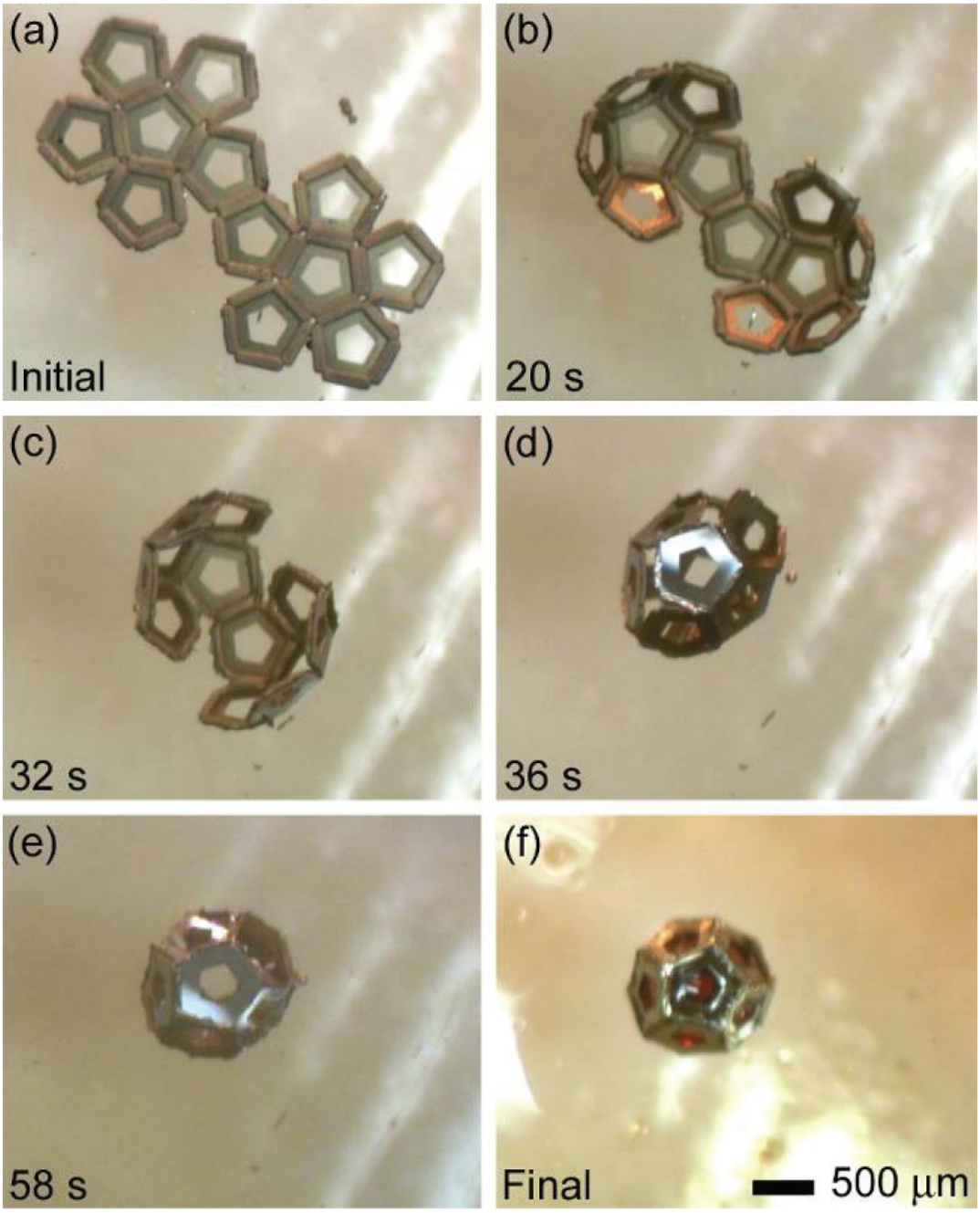

Figure 4. Video snapshots featuring the hierarchical self-assembly of a 500 µm dodecahedron

(a) Initial 2D dodecahedron template. (b) The two symmetrical halves of the net assemble simultaneously. (c) The central hinge begins to fold, resulting in the two hemi-dodecahedra which approach each other. (d–e) Although it appears that each hemi-dodecahedron has folded to different extents, the locking hinges self-correct the orientation to achieve the desired, optimal configuration. (f) The final self-assembled dodecahedron.

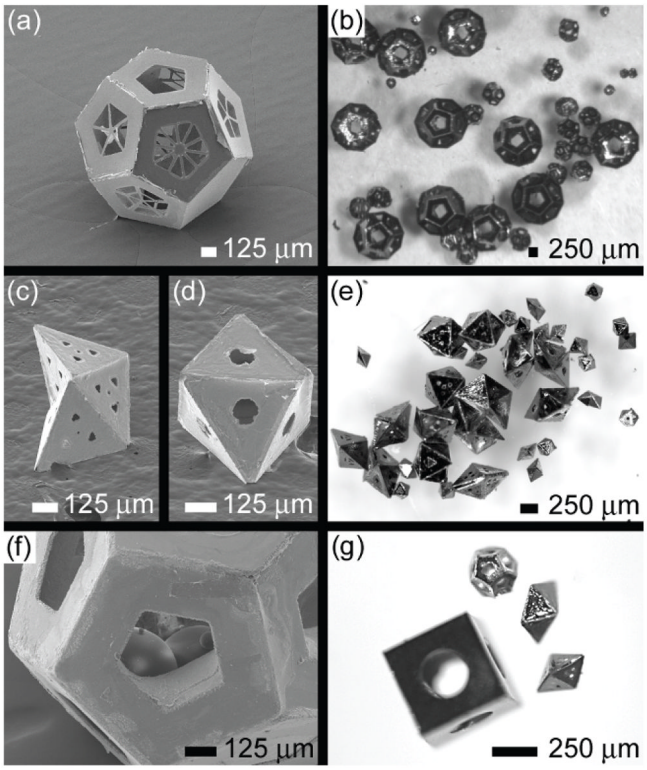

Figure 5. Process Versatility

(a) SEM image of a folded 3D dodecahedron container featuring anisotropic surface patterning (i.e. different specific desired patterns on each panel). (b) Optical image of numerous 100 μm, 200 μm and 500 μm (panel edge length) dodecahedra. (c–d) SEM images of folded 3D octahedral containers in boat and regular configurations, respectively. (e) Optical image of numerous 200 μm and 500 μm sized octahedra. (f) SEM image of a bead encapsulated within a dodecahedral shaped container. (g) Optical image of a self-assembled 500 μm cube, two 200 μm octahedra in different configurations, and a 100 μm dodecahedron.